Biophysical Review

Time-Resolved Fluorescence in Lipid Bilayers: Selected Applications and Advantages over Steady State

Mariana Amaro,[1] Radek Šachl,[1] Piotr Jurkiewicz,[1] Ana Coutinho,[2,3] Manuel Prieto,[2] and Martin Hof[1,*]
[1]Department of Biophysical Chemistry, J. Heyrovský Institute of Physical Chemistry of the Academy of Sciences of the Czech Republic, v.v.i., Prague, Czech Republic; [2]Centre for Molecular Chemistry and Physics and Instituto de Nanociência e Nanotecnologia, Instituto Superior Técnico and [3]Departamento Química e Bioquímica, Faculdade de Ciências, Universidade de Lisboa, Lisbon, Portugal

ABSTRACT Fluorescence methods are versatile tools for obtaining dynamic and topological information about biomembranes because the molecular interactions taking place in lipid membranes frequently occur on the same timescale as fluorescence emission. The fluorescence intensity decay, in particular, is a powerful reporter of the molecular environment of a fluorophore. The fluorescence lifetime can be sensitive to the local polarity, hydration, viscosity, and/or presence of fluorescence quenchers/energy acceptors within several nanometers of the vicinity of a fluorophore. Illustrative examples of how time-resolved fluorescence measurements can provide more valuable and detailed information about a system than the time-integrated (steady-state) approach will be presented in this review: 1), determination of membrane polarity and mobility using time-dependent spectral shifts; 2), identification of submicroscopic domains by fluorescence lifetime imaging microscopy; 3), elucidation of membrane leakage mechanisms from dye self-quenching assays; and 4), evaluation of nanodomain sizes by time-resolved Förster resonance energy transfer measurements.

Fluorescence techniques are well known for their high sensitivity, up to single-molecule detection—a characteristic of paramount relevance, particularly in membrane biophysics. This sensitivity has allowed fluorescence experiments to contribute significantly to contemporary understanding of the organization and dynamics of biomembranes. Fluorescence experiments can be carried out as time-resolved (TR) measurements or using the more common steady-state (SS) approach employing standard spectrofluorometer. TR methods can retrieve the fluorescence intensity decay, which contains information about the molecular environment of a fluorophore that can be related to the system dynamics and topology. An important advantage of TR compared to SS measurements is that they are less or not affected by artifacts (e.g., light scattering, inner filter effects, etc.). In addition, single photon timing (the most popular TR approach) has become increasingly more accessible due to the development of less expensive pulsed light sources. In contrast, all SS fluorescence measurements share an intrinsic disadvantage that stems from the loss of information caused simply by the integration of intensity over time.

This mini-review describes recent examples from the literature where TR methods unveiled information about the system under study that would not be accessible from SS data. Specifically, it will be shown how TR fluorescence measurements allow for quantitative recovery of detailed information regarding the lipid bilayer structure and dynamics, lateral and transversal organization of fluorescently labeled molecules in lipid membranes, and membrane permeabilization mechanisms. For other valuable fluorescence approaches employed in membrane studies, such as diphenylhexatriene fluorescence anisotropy to study membrane order and rotational dynamics (1), pyrene excimer formation to evaluate lateral diffusion (2), or fluorescence quenching measurements to assess membrane heterogeneities (3), the reader is directed to seek other reviews.

Determining polarity and mobility in lipid bilayers using time-dependent fluorescence shift: focus on Laurdan and comparison with generalized polarization

Polarity and mobility are very important properties that strongly vary along the z axis of lipid bilayers. Relevant information about these parameters has been gained by performing nuclear magnetic resonance (4,5), neutron and x-ray diffraction (5,6), and electron spin resonance (7) measurements using model membrane systems. Time-dependent fluorescence shift (TDFS) measurements can also be used to explore the transversal gradients of hydration and mobility in lipid bilayers because the fluorescence emission of a fluorophore can be sensitive to the dynamics and polarity of its immediate vicinity. TDFS experiments are based on the ultrafast change in the dipole moment of a fluorophore upon electronic excitation, to which its solvation shell must respond. This dipolar relaxation causes a time-dependent shift of the peak maxima $\nu(t)$ of the time-resolved emission spectra, which are reconstructed from a set of wavelength dependent fluorescence decays (8). The analysis of $\nu(t)$ reveals independently information on the polarity and

Submitted August 11, 2014, and accepted for publication October 29, 2014.
*Correspondence: martin.hof@jh-inst.cas.cz
Editor: Heiko Heerklotz.

0006-3495/14/12/2751/10 $2.00
http://dx.doi.org/10.1016/j.bpj.2014.10.058

the mobility of the solvation shell, a unique advantage of this technique. The total amount of fluorescence shift $\Delta\nu$ (Eq. 1) is proportional to polarity (9), whereas the TDFS kinetics, expressed as the mean integrated relaxation time τ_r (Eq. 2), depends on solvent viscosity (10):

$$\Delta\nu = \nu(0) - \nu(\infty), \tag{1}$$

$$\tau_r = \int_0^\infty \frac{\nu(t) - \nu(\infty)}{\Delta\nu} dt. \tag{2}$$

Here, $\nu(0)$ and $\nu(\infty)$ correspond, respectively, to the spectral maxima at time zero (Frank–Condon state) and at time infinity (fully relaxed state) after excitation. The steep hydration gradient along the z axis of lipid bilayers governs the readout parameters $\Delta\nu$ and τ_r of an individual membrane probe (11). Thus, precise knowledge of the transversal location of the fluorescent probe is crucial for mapping the information gained in these studies with respect to the z axis of the lipid bilayer (8,12).

Here we will focus on using Laurdan (6-lauroyl-2-dimethylaminonaphthalene) for TDFS experiments (13). The increase in dipole moment upon Laurdan excitation has been reported to be as large as 20 d (13) or, more recently, of 13 d (14). This results in a strong dependence of its fluorescence emission on the polarity and viscosity of the solvent used, and a large Stokes shift of up to 7400 cm^{-1} in lipid bilayers (15). For the interpretation of Laurdan TDFS experiments in lipid membrane studies, it is important to note the following:

1. In the liquid crystalline phase, TDFS occurs exclusively on the nanosecond timescale (16);
2. TDFS in bulk water is ~1000 times faster (9);
3. The residence time of bound water molecules within phospholipid headgroups is considerably longer than the fluorescence lifetime of the probes (~60 ns) (4); and
4. TDFS is theoretically attributed to the collective relaxation of the dye environment, and does not provide information on exchange of single water molecules (9,17).

Regarding Laurdan transverse location, all-atom classical molecular-dynamics simulations yielded mean distances of its fluorophore from a DOPC (1,2-dioleoyl-*sn*-glycero-3-ethylphosphocholine) bilayer center in the liquid crystalline phase of 12.3 ± 2.1 Å and 13.5 ± 2.5 Å for the ground and excited states of Laurdan, respectively (relocation occurs on the nanosecond timescale) (18). Parallax quenching experiments with spin-labeled lipids confirmed that Laurdan is located near the DOPC *sn*-1 carbonyls (19). Furthermore, the wavelength-dependence of the quenching also showed that Laurdan moves ~2 Å toward aqueous media within its fluorescence lifetime. Taking all the above facts together, one can conclude that Laurdan τ_r reflects the rearrangement of hydrated *sn*-1 carbonyls of a lipid bilayer in the liquid crystalline phase, whereas $\Delta\nu$ mirrors the polarity, which is related to the hydration level of *sn*-1 carbonyls.

Laurdan was chosen here as an example due to its widespread use in model and cell membranes studies to assess membrane order/hydration (20). Laurdan presents distinct maxima emission wavelengths in the liquid crystalline L_α (490 nm) and in the gel L_β (440 nm) phases of a lipid bilayer. This has been used by Parasassi et al. (15) to define the so-called generalized polarization function (*GP*),

$$GP = \frac{I_{440} - I_{490}}{I_{440} + I_{490}}, \tag{3}$$

where I_{440} and I_{490} represent the SS fluorescence intensities emitted at these characteristic wavelengths. *GP* is an empirical steady-state ratiometric parameter that is defined in a similar way to the classical fluorescence polarization, hence the name. Its origin is based on a simple two-state model of dipolar relaxation, which assumes that Laurdan emits exclusively from either the unrelaxed Frank-Condon state or the fully relaxed state (21). This approximation produces easy-to-obtain results that have proven to be useful in characterizing lipid bilayer phases (20,22), e.g., allowing detection of phase coexistence (15) or cholesterol presence (23).

Laurdan (and analogs Prodan and Patman) TDFS has been used to investigate many biophysical aspects of model membranes, the majority of which have been summarized in three reviews (8,16,24). To illustrate the potential of TDFS measurements and its SS sister *GP* approach, we will discuss two selected cases.

1. A simple temperature dependence.
2. The incorporation of transmembrane peptides.

Temperature dependence of $\Delta\nu$, τ_r, and *GP* in 1,2-dimyristoyl-*sn*-glycero-3-phosphocholine large unilamellar vesicles

As described above, $\Delta\nu$ and τ_r, are well-defined parameters directly correlated with the local polarity and mobility experienced by the fluorescent probe. However, this only holds true when reasonable estimates of $\nu(0)$ and $\nu(\infty)$ are available. The value $\nu(0)$ can be calculated by time-zero estimation for the majority of used probes (8). On the other hand, if part of the reorientation dynamics is slower than the lifetime of the dye, then $\nu(\infty)$, intrinsically, cannot be determined. A typical example, where fluorescence occurs before the solvation shell response is complete, is the fluorescence of Laurdan in 1,2-dimyristoyl-*sn*-glycero-3-phosphocholine (DMPC) bilayers below the phase-transition temperature ($T_m = 24°C$). In such conditions, $\Delta\nu$ and τ_r values as well as *GP* have to be understood as empirical parameters with limited physical meaning (*blue points* in Fig. 1).

At greater than T_m, the overall TDFS kinetics is faster than Laurdan fluorescence and thus $\nu(\infty)$ can be accurately determined. The value $\Delta\nu$ increases with the rising temperature until reaching a saturation level that is indicative of the full hydration of the *sn*-1 carbonyls. The τ_r values follow an Arrhenius-like behavior, which indicates the increased

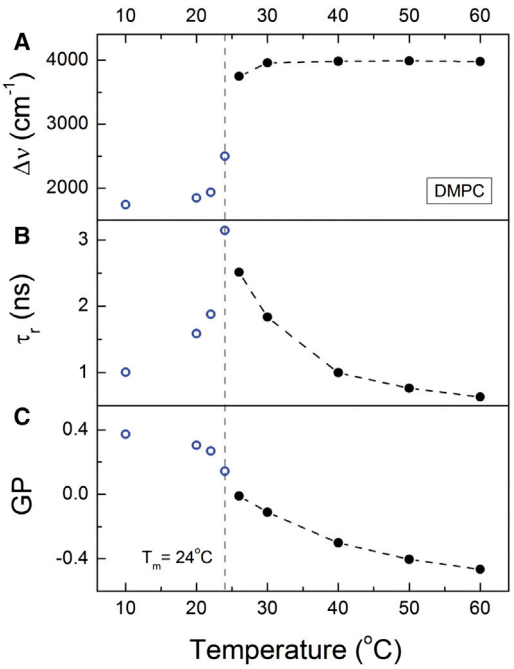

FIGURE 1 Time-resolved and steady-state fluorescence parameters for Laurdan embedded in DMPC LUVs as a function of temperature. (*A*) Total spectral shift and (*B*) integrated relaxation times obtained from analysis of time-resolved emission spectra. (*C*) Excitation *GP* calculated from the steady-state spectra. (*Open blue circles*) Data points obtained below DMPC main phase transition temperature (T_m, marked with a *vertical dashed line*), which are only crude estimates of the true values because of the limited fluorescence lifetime of the probe; see the text for details. Adapted from Jurkiewicz (25). To see this figure in color, go online.

mobility of the hydrated *sn*-1 carbonyls with increasing temperature. As can be seen in Fig. 1 (see also Jurkiewicz (25)), in L_α phase *GP* correlates with τ_r rather than with $\Delta\nu$. This means that *GP* reflects predominantly the mobility of the hydrated *sn*-1 carbonyls and not the extent of hydration of the L_α lipid bilayer.

Impact of transmembrane peptides on $\Delta\nu$, τ_r, and *GP* in 1-palmitoyl-2-oleoyl-phosphatidylcholine large unilamellar vesicles

Upon considering Laurdan applications in living cells, it is of interest to know how *trans*-membrane peptides (TMPs) can influence its TDFS parameters, $\Delta\nu$ and τ_r, respectively. To this end, the effect of two model peptides,

LAT (Glu-Glu-Ala-Ile-Leu-Val-Pro-Ser-Val-Leu-Gly-(Leu)4-Pro-Ile-Leu-Ala-Met-Leu-Met-Ala-Leu-Ser-Val-His-Ser-His-Arg-NH2)

and

LW21 (Gly-Leu-Leu-Asp-Ser-(Lys)2-(Trp)2-(Leu)8-Ala-(Leu)8-(Trp)2-(Lys)2-Phe-Ser-Arg-Ser-NH2),

on Laurdan fluorescence was investigated in 1-palmitoyl-2-oleoyl-phosphatidylcholine (POPC) large unilamellar vesicles (LUVs) at 20°C (26). LAT and LW21 peptides mimic transmembrane domains of integral membrane proteins.

The presence of the peptides led to a substantial increase in all of the discussed parameters: τ_r, $\Delta\nu$, *GP*. The increase of τ_r means that the insertion of the peptide restricts local dynamics of the hydrated carbonyls. The increase of $\Delta\nu$ indicates increased polarity, possibly due to the presence of the peptide in the vicinity of the probe. The increase of *GP* cannot be caused by increased polarity (a decrease in *GP* would be expected in such a case). Therefore, *GP* does not give information on changes in polarity or hydration in this case, whereas $\Delta\nu$ is able to sense an increase in polarity. In accordance with Case 1 above, the TDFS data show that the increase in *GP* reflects the lower mobility of the chromophore environment upon incorporation of the TMPs in the membrane.

The simpler implementation of Laurdan *GP*, as compared to TDFS measurements, is the base of its success in membrane biophysics. *GP* is also applicable to fluorescence microscopy, where it can easily be determined for each single pixel. An equivalent determination of the whole time-resolved emission spectra would be very demanding. However, the given examples demonstrate that Laurdan TR parameters, $\Delta\nu$ and τ_r, yield independent information on polarity and mobility at the *sn*-1 carbonyls level, in contrast to *GP*. In gel phases, TDFS physical interpretation is hampered because $\nu(\infty)$ cannot be determined and $\Delta\nu$ and τ_r (as well as *GP*) become empirical parameters. For most examined cases, e.g., interactions of monovalent cations with negatively charged bilayers (27) or lipid oxidation (28), increases in $\Delta\nu$ indicate greater hydration with a concomitant higher mobility of *sn*-1 carbonyls (8,16). However, the TMPs example illustrates that in specific cases one can observe hindered mobility along with increased polarity. Other such examples include the effect of NaBr in cationic bilayer (29), or interaction of β-blockers with POPC (30). For liquid crystalline phases, the data demonstrate that *GP* is an indicator of phospholipid headgroup mobility and not, as often found in the literature, of "extent of water penetration" (31).

Detecting submicroscopic domains in lipid bilayers using fluorescence lifetime imaging: focus on NBD-lipid analogs

Whereas TR bulk measurements are useful due to their statistical accuracy, here we would like to highlight the use of fluorescence lifetime imaging microscopy (FLIM) to detect lateral heterogeneities in lipid bilayers. FLIM combines microscopy with fluorescence decay acquisition over the image, thus adding the extra dimension of spatial resolution to a study, albeit with a lower degree of statistical precision. In 2008, Stöckl et al. (32) used a combination of the probe NBD (*N*-(7-nitrobenz-2-oxa-1,3-diazol-4-yl)) and the FLIM technique to detect submicroscopic domains in lipid bilayers. This finding is worthy of note, because submicroscopic

domains are usually detected through the use of more complex methods such as, e.g., small-angle neutron scattering (33), electron spin resonance (34,35), and Förster resonance energy transfer (FRET) experiments (35,36). Such methods are complex both at the level of execution and data analysis (see last section of this review for more details on FRET).

The previous section discussed a fluorescent probe displaying strong dipole-moment changes upon excitation. In contrast, the NBD fluorophore highlighted in this section has very different photophysical characteristics. NBD derivatives show a random Stokes shift variation with solvent polarity (37) that renders them unsuitable for TDFS studies. This is in-line with the estimated small transition dipole moments of 0.8 d or 1.8 d (37,38). However, NBD has other interesting photophysical characteristics, such as its fluorescence quantum yield and lifetime, which depend strongly on the solvent. The latter parameter ranges from values between 4 and 10 ns in 17 examined solvents (37), and in water it drops to 1 ns.

The labeling of NBD-lipid analogs can be done through the secondary amine to attach the fluorophore either to the *sn*-2 acyl chain or to the polar headgroup of various lipids (see Fig.1 in Haldar and Chattopadhyay (39)). Interestingly, even for the tail-labeled lipid analogs the chromophore resides at the upper acyl-chain/glycerol backbone area. NBD loops or snorkels to the water/lipid interface due to its polarity and the acyl-chain flexibility (40–42). The combination of the location of NBD at the membrane water/lipid interface (an area known to have a steep hydration gradient along its *z* axis) with the high sensitivity of its fluorescence lifetime to the water content around the fluorophore makes it a valuable membrane sensor that can be used to probe membrane lateral organization, as shown below.

Stöckl et al. have found (32) that the lifetime of C6-NBD-lipids is sensitive to the presence of a liquid-disordered (L_d) or liquid-ordered (L_o) lipid lamellar phase. Namely, the longer lifetime of C6-NBD-PC (PC, phosphatidylcholine) was ~7 ns in several different L_d phase membranes, and ~12 ns in vesicles of L_o phase. C6-NBD-PC clearly reported the phase coexistence when in bilayers displaying microscopic phase separation (Fig. 2 *C*). The fluorescence lifetime histograms recovered from the FLIM images exhibited without doubt the presence of the two peaks. More importantly, FLIM has the capacity of detecting domains below the optical resolution if they are sufficiently long-lived (at least three times the dye fluorescent lifetime) (32). The lifetime histograms can report their existence and in fact, the two distinct long lifetimes of C6-NBD-PC were also identifiable in compositions known to have submicroscopic phase separation (Fig. 2 *D*) (32,43).

Using FLIM to detect submicroscopic domain coexistence in membranes is a simpler and more straightforward approach in comparison to the other frequently used methods. The concept is also based on using only one fluorescent probe, which is another advantage. As a final note, FLIM experiments with C6-NBD-PC on cellular membranes yielded lifetime histograms that displayed broad distributions (32). This finding is in line with the idea that coexisting phases in cellular membranes are rather similar in their

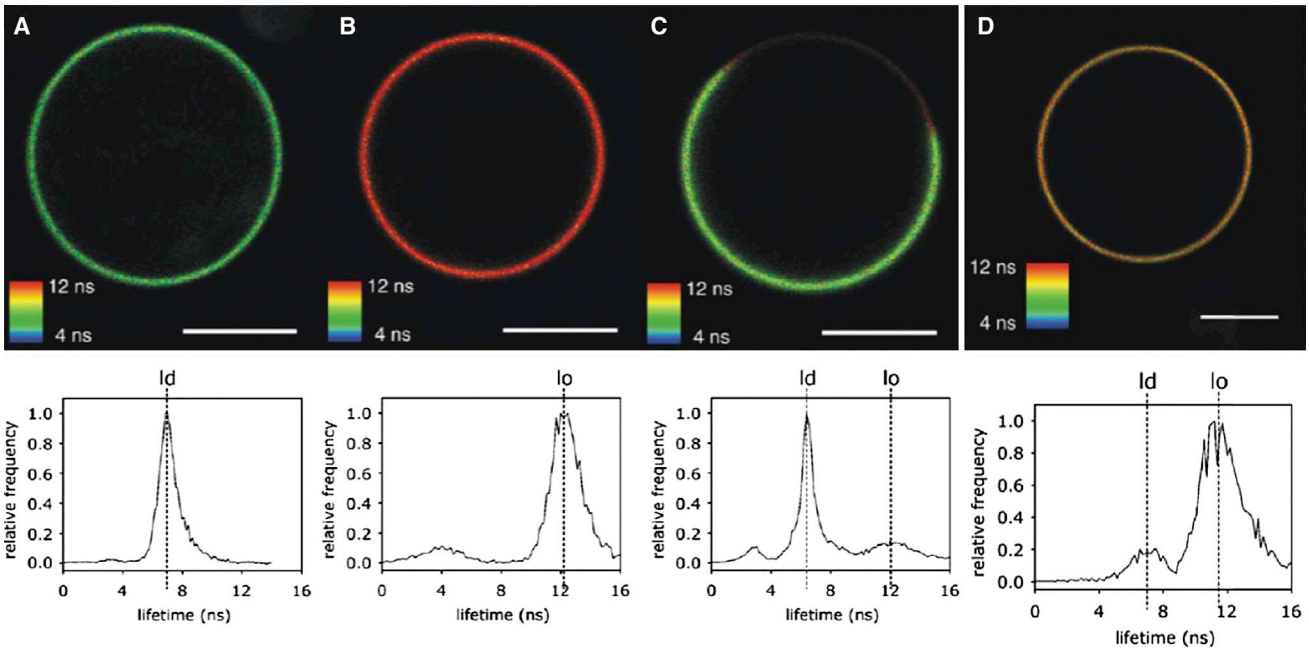

FIGURE 2 (*Top row*) Average lifetime of C6-NBD-PC in giant unilamellar vesicles prepared from (*A*) DOPC, liquid-disordered phase (*Ld*); (*B*) DOPC/Sphingomyelin/Cholesterol = 1/1/8, liquid-ordered phase (*Lo*); (*C*) DOPC/Sphingomyelin/Cholesterol = 1/1/1, *Ld* and *Lo* phase coexistence; and (*D*) DOPC/Sphingomyelin/Cholesterol = 4/2/4, submicroscopic phase coexistence. (*Bars*) 10 μm. (*Bottom row*) Respective lifetime histograms, normalized to 1 at maximum. Figure adapted from Stöckl and Herrmann (43) To see this figure in color, go online.

nature, whereas in model systems the differences are more extreme (44,45).

Determining membrane permeabilization mechanisms using TR measurements of calcein

Membrane leakage assays are extensively used to study membrane permeabilization mechanisms not only in model lipid systems (46), but also in living cells (47). The typical SS experiment consists of enclosing a self-quenching dye inside lipid vesicles and detecting the increase in fluorescence intensity over time as the dye is progressively released and diluted by the action of a membrane-permeabilizing molecule. This assay allows us to measure the activity of the permeabilizing agent, which is related to the dye efflux, E (48,49). The release of the encapsulated contents can occur by an all-or-none mechanism, where a fraction of vesicles remains intact whereas others lose all their contents, or by a graded mechanism, where all the vesicles release a fraction of their content. It is necessary to know its efflux mechanism to correctly model and analyze the efflux kinetics of the entrapped dye (50). This is also an important feature that must be known to propose a mechanism of action for the permeabilizing agent (46,51,52).

Fluorescence microscopy has been used to image individual lipid vesicles and follow their leakage kinetics through SS intensity measurements (53,54). Although highly informative, this methodology lacks the high statistical accuracy of bulk measurements. On the other hand, fluorescence correlation spectroscopy can be used for tracking leakage of fluorescent molecules from liposome ensembles (55); however, access to a fluorescence microscope can be limited and in fact, the traditional SS spectroscopic techniques remain the simplest and most accessible way to follow leakage kinetics in ensembles.

To ascertain the release mechanism using a SS assay, one has to do additional experimental work to determine the quenching factor Q of the dye that remains encapsulated. This involves physically removing the released dye or titrating it with a quencher (56). The requenching technique requires knowledge of the quenching mechanism. Also, quencher can diffuse into the vesicles in the case of graded leakage. Details on pore kinetics can be obtained by further analysis of the SS E with analytical (57–59) or numerical methods (60). However, the SS calculated E does not necessarily correspond to the true percentage of dye released, especially in the case of graded leakage, as already pointed out in 1995 by Ladokhin et al. (56). E values calculated from SS data are not accurate when a graded leakage mechanism is operative because they are affected by the increase in quantum yield of the entrapped dye as its internal concentration decreases. The fluorescence intensity of the entrapped dye increasingly contributes to the overall SS signal, which no longer reflects the true percentage of released content. The release of dye is not necessarily a linear phenomenon, and, therefore, it is not straightforward to model the increase of quantum yield when calculating E.

Fluorescence lifetime measurements have been proposed for long time as a solution to the problem described above (56). In 2009, the idea has been shown to work with calcein (61). For calcein, static quenching is far less significant than dynamic quenching (61), therefore calcein should display different lifetime responses for graded versus all-or-none leakage. In the all-or-none case, lifetimes of free and entrapped dye remain the same whereas their fractions vary as the dye is released (46). For graded leakage, not only the fractions of free/entrapped dye vary but also the lifetime of the entrapped dye increases as its concentration is lowered by the partial dye release (61). TR leakage assays can also be used to make more-accurate calculations of E. As Patel et al. (61) have shown, the contribution of the dye that remains entrapped can be quantified and corrected for, using the preexponential factors recovered from fitting the decays of the fluorescence intensity.

TR leakage assays have the advantage of providing more information for less experimental work. They allow direct determination of leakage mechanism without requiring removal of leaked dye, in contrast to SS measurements, and calculation of more accurate values of E. Another advantage of the TR leakage assay is that, in addition to directly distinguishing the release mechanism, it also allows assessment of the degree of heterogeneity of graded leakage (Fig. 3).

Measuring domain sizes and distances in lipid bilayers using time-resolved FRET

Time-resolved FRET (TR-FRET) is a powerful tool for determining nanodomain sizes, measuring intra- and

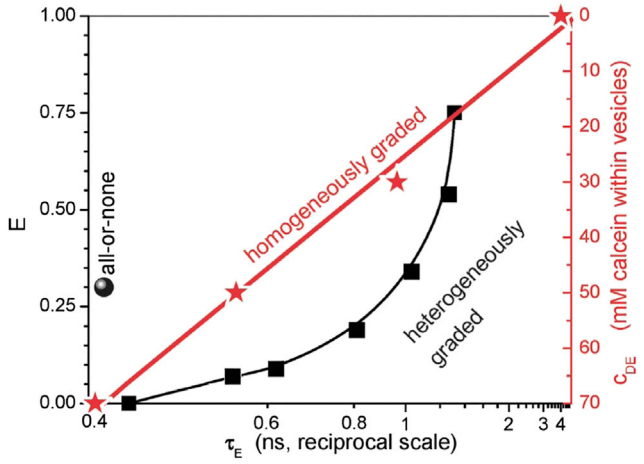

FIGURE 3 (*Left axis*) Correlation of efflux E with lifetime of entrapped calcein dye, τ_E. (*Right axis*) Correlation of local dye concentration c_{DE} (*stars*) with lifetime of entrapped dye, τ_E. From $E(\tau_E)$, leakage can be assigned to all-or-none (*black sphere*) or homogeneous/heterogeneous graded leakage (*squares*). Figure adapted from Patel et al. (61). To see this figure in color, go online.

interbilayer distances and locating fluorescent probes within a lipid bilayer. The rate constant for the FRET interaction between an isolated donor-acceptor (D-A) pair is proportional to the inverse sixth power of the distance between them, allowing easy determination of distances at the nanometer scale (62). However, in membrane studies it is not possible to define a unique D-A distance at variance with this simpler situation. Instead, a distribution function of D-A distances of A around D must be considered. The Baumann-Fayer (BF) model (63) describes the survival probability of the excited D molecules when D and A are uniformly distributed in a lipid bilayer. However, there are no analytical solutions for quantitative description of complex geometrical arrangements such as, e.g., small domains and pores in lipid bilayers. Numerical simulation must then be used to obtain quantitative information about such systems.

Determining domain sizes

As of this writing, only a few methods are capable of detecting nanometer domains in lipid bilayers. Atomic force microscopy (AFM) provides high-resolution images that can be used to measure domain sizes and construct histograms (64). However, AFM requires use of supported lipid bilayers, and lipid domains can be affected by lipid-substrate interactions. Stimulated emission depletion spectroscopy is capable of resolving structures as small as ~20 nm and can contain dynamic information when in the fluorescence correlation regime (65). Nonetheless, this is still a complex and not-widespread technique. Domain size determination using TR-FRET is less straightforward because of the complexity of the analytical models, which must take into account the specific system topology. The advantage of this technique is, however, its very high resolution at measuring on the nanoscale.

The ability of TR-FRET to determine domain sizes on free-standing bilayers strongly depends on D and A molecules' relative affinities to domains and remaining bilayer (66). As a rule of thumb, the more the D and A molecules' distribution coefficients (K_D and K_A, respectively) deviate from 1, with D and A having opposite phase preference, the smaller the domain sizes one can determine (66). It has been shown that domains smaller than the Förster radius (R_0) or >15–20 R_0 approach the resolution limit of TR-FRET (67).

The BF model on its own can only ascertain whether labeled molecules form clusters in a bilayer. Marushchak et al. (36) have shown that when clusters exist, the BF model yields overestimated values for the surface concentration of *A* in comparison to the expected ones (which can be calculated from the known probe/lipid ratio). A quantitative method developed by de Almeida et al. (67), Loura and Prieto (68), and Loura et al. (69) has been a frequently used approach for assessing domain sizes that relies to some extent on the BF model. The method models the TR data as a linear combination of the D-molecule decays in two distinct phases, each described by the BF model. The surface concentrations obtained by fitting can be used to estimate K_D and K_A between the two phases. Not surprisingly, with decreasing domain sizes the estimated K_D and K_A deviate from the partition coefficients obtained through complementary independent methods (69). This occurs because the model neglects FRET across the phase separation boundary (no interdomain transfer) and, as the domain size decreases, the interdomain transfer becomes significant. This assumption is very critical, but it allows roughly estimating the size of domains. Through comparison of the experimental and estimated partition coefficients, the following limits on the rafts domain sizes in model systems were set to:

1. Domains radius $R < 20$ nm for low cholesterol content;
2. 20 nm $< R <$ 15–20 R_0 for intermediate cholesterol content; and
3. $R >$ 15–20 R_0 for >30 mol % cholesterol, where FRET across the phase separation boundary can be neglected (67).

Higher precision in domain size estimation can in fact be achieved using TR-FRET combined with Monte Carlo (MC) simulations (70,71). The TR-FRET/MC method accounts for FRET across the phase separation boundary. It relies on generating a simulated decay of a D molecule undergoing FRET. The simulated decay is matched to the experimental one by varying the domain radius and the number of domains (Fig. 4). Because several combinations of domain sizes and numbers can yield the same FRET efficiency but different decay shapes, the TR-FRET/MC approach is superior to the SS-FRET method and should be preferred. TR-FRET/MC has been demonstrated to be capable of determining sizes of L_o nanodomains stabilized by Cholera toxin subunit B (71) and of small (5–7 nm radius) ganglioside GM_1 clusters in DOPC/Cholesterol bilayers (72), which correspond well to AFM-determined sizes (64). The method provides not only domain sizes but also the fraction of bilayer area occupied by the domains. This can be useful in the characterization of domains, as shown for the case of GM_1 clusters (72). In the referred work, the determined occupancy of up to 40% of the bilayer surface by GM_1 clusters, whereas the total GM_1 amount did not exceed 4%, allowing us to conclude that DOPC and Cholesterol were major constituents of the clusters.

Up to this point, it was assumed that D and A molecules were distinct chromophores (hetero-FRET). A simpler experimental situation involves the occurrence of FRET between photophysically identical fluorophores (homo-FRET or donor-donor energy migration). Homo-FRET can only be monitored by quantifying its effect on the depolarization of fluorescence (fluorescence anisotropy). Homo-FRET studies performed employing SS methodologies only allow

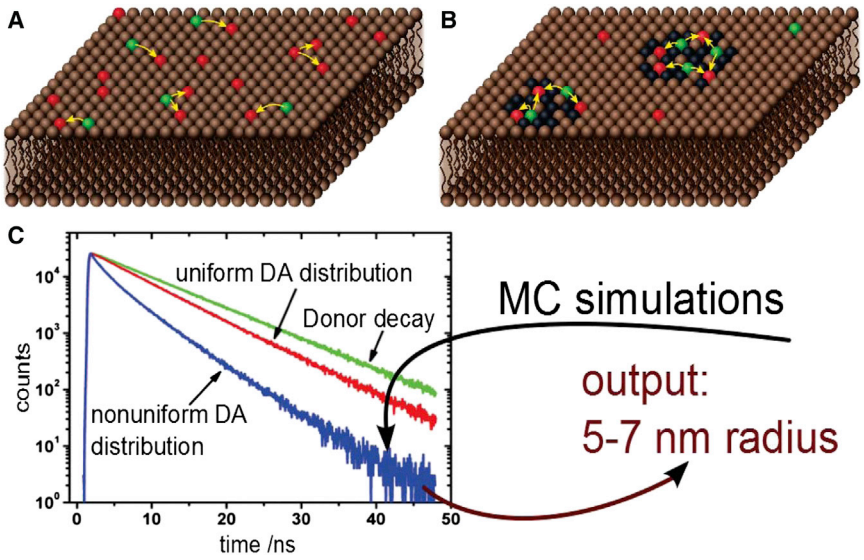

FIGURE 4 Illustration of FRET concept as used in Sachl et al. (72). (*Green* and *red spheres*) Donor (D) and acceptor (A) molecules labeled-ganglioside GM_1, respectively. (*A*) Homogeneous distribution of D and A molecules; (*B*) D and A molecules, both with increased affinity to GM_1 clusters (*darker areas*). (*C*) MC simulations calculate D molecule fluorescence decay and optimize domain size/domain number until it matches the experimentally obtained decay. To see this figure in color, go online.

detecting the formation of domains. With SS, the relative decrease in fluorescence anisotropy upon increasing the surface density of fluorophores is measured. The lipid segregation is inferred from the deviations of the relative decrease in anisotropy from the one expected for a statistically random distribution on the two-dimensional plane of the membrane (homo-FRET due to concentration-depolarization) (e.g., Castro et al. (73)).

As with hetero-FRET, TR experiments can provide more information, but it is difficult to rationalize the extent of depolarization caused by homo-FRET. This is due to the reversibility of the transfer process between identical fluorophores and to the possible coupling between energy migration and the rotational diffusion of the molecule. However, coupling can usually be ignored in lipid bilayers where each donor is surrounded by several randomly oriented acceptors. Such conditions mimic the static isotropic regime for which rotational motions are not coupled with FRET (70). If the coupling can be ignored, the TR anisotropy decay for randomly surface-distributed molecules in the presence of homo-FRET can be described semiempirically (74). Although not directly related to lipid domain formation, TR homo-FRET measurements have also been used to study the oligomer formation of peptides and proteins in lipid membranes (75). In this case, TR measurements are the best way to verify the occurrence of homo-FRET by detection of a much faster anisotropy relaxation to the characteristic plateau value (75). The theoretical framework relating the SS fluorescence anisotropy to oligomer stoichiometry has been derived by Runnels and Scarlata (76) and the exact solution for TR homo-FRET between a pair of like fluorophores is also available (77). Quantitative information about the membrane-bound oligomer size can be obtained through modeling the decrease of anisotropy upon varying the photobleaching level or the fractional labeling of the sample (78), even in the presence of an additional partition equilibrium (79).

Determining distances

Energy transfer to the other membrane leaflet (inter-FRET contribution) must also be considered in FRET models because the membrane thickness is comparable to the typical R_0. In fact, the extra dimension of the interleaflet contribution to FRET is what allows the determination of the depth of molecules in membranes. For example, a transverse distance of 27 Å between the chromophore of tail-labeled lipid-analogs was measured with the use of one FRET reference probe whose vertical position in the bilayer was known (80). Two straightforward applications of this method are as follows:

1. Measurement of bilayer thickness, using a FRET pair where the probes reside at the water/lipid interface (36); and
2. Detection and characterization of multibilayer stacking upon interaction of cationic peptides (81) or proteins (82) with anionic membranes.

The TR-FRET approach has several advantages over the popular SS parallax quenching (PQ) method (80). TR-FRET only requires one reference probe, whereas PQ needs two transversally well-separated probes. TR-FRET assures better distance resolution and the choice of reference probes with known localization is broader. In addition, because the SS PQ method is based upon static quenching, it requires using high quencher concentrations and thus involves higher membrane perturbation.

In summary, TR-FRET is a very powerful technique for the measurement of sizes and distances in lipid bilayers. With it, it is possible to determine distances that are as small

as a few nanometers. This allows sizing nanoheterogeneities in membranes, such as lipid domains and protein aggregates, and the spatial localization of fluorophores (which, for example, permits the determination of membrane thickness).

The authors thank Luís M. S. Loura and Suzanne Fery-Forgues for discussions about the transition dipole moment and the photophysics of NBD, and Agnieszka Olzyńska for the preparation of Fig. 1.

The authors from J. Heyrovský Institute acknowledge financial support from the Czech Science Foundation (under grant No. 14-03141J) and the Ministry of Education, Youth and Sports of the Czech Republic (under grant No. LH13259 KONTAKT). M.H. acknowledges the Academy of Sciences for the Praemium Academie award. M.P. acknowledges Project No. RECI/CTM-POL/0342/2012.

REFERENCES

1. Lentz, B. R. 1993. Use of fluorescent probes to monitor molecular order and motions within liposome bilayers. *Chem. Phys. Lipids.* 64:99–116.
2. Galla, H.-J., and W. Hartmann. 1980. Excimer-forming lipids in membrane research. *Chem. Phys. Lipids.* 27:199–219.
3. Duportail, G. 2005. Raft microdomains in model membranes as revealed by fluorescence quenching. *In* Fluorescence Spectroscopy in Biology. M. Hof, R. Hutterer, and V. Fidler, editors. Springer, Berlin, Germany, pp. 133–149.
4. Westlund, P.-O. 2000. Line shape analysis of NMR powder spectra of ^2H_2O in lipid bilayer systems. *J. Phys. Chem. B.* 104:6059–6064.
5. Gawrisch, K., H. C. Gaede, …, S. H. White. 2007. Hydration of POPC bilayers studied by ^{1}H-PFG-MAS-NOESY and neutron diffraction. *Eur. Biophys. J.* 36:281–291.
6. Tristram-Nagle, S., and J. F. Nagle. 2004. Lipid bilayers: thermodynamics, structure, fluctuations, and interactions. *Chem. Phys. Lipids.* 127:3–14.
7. Marsh, D. 2001. Polarity and permeation profiles in lipid membranes. *Proc. Natl. Acad. Sci. USA.* 98:7777–7782.
8. Jurkiewicz, P., J. Sýkora, …, M. Hof. 2005. Solvent relaxation in phospholipid bilayers: principles and recent applications. *J. Fluoresc.* 15:883–894.
9. Horng, M. L., J. A. Gardecki, …, M. Maroncelli. 1995. Subpicosecond measurements of polar solvation dynamics: Coumarin 153 revisited. *J. Phys. Chem.* 99:17311–17337.
10. Richert, R., F. Stickel, …, M. Maroncelli. 1994. Solvation dynamics and the dielectric response in a glass-forming solvent: from picoseconds to seconds. *Chem. Phys. Lett.* 229:302–308.
11. Sýkora, J., P. Kapusta, …, M. Hof. 2002. On what time scale does solvent relaxation in phospholipid bilayers happen? *Langmuir.* 18:571–574.
12. Demchenko, A. P., Y. Mély, …, A. S. Klymchenko. 2009. Monitoring biophysical properties of lipid membranes by environment-sensitive fluorescent probes. *Biophys. J.* 96:3461–3470.
13. Weber, G., and F. J. Farris. 1979. Synthesis and spectral properties of a hydrophobic fluorescent probe: 6-propionyl-2-(dimethylamino)naphthalene. *Biochemistry.* 18:3075–3078.
14. Cwiklik, L., A. J. Aquino, …, H. Lischka. 2011. Absorption and fluorescence of PRODAN in phospholipid bilayers: a combined quantum mechanics and classical molecular dynamics study. *J. Phys. Chem. A.* 115:11428–11437.
15. Parasassi, T., G. De Stasio, …, E. Gratton. 1990. Phase fluctuation in phospholipid membranes revealed by Laurdan fluorescence. *Biophys. J.* 57:1179–1186.
16. Jurkiewicz, P., L. Cwiklik, …, M. Hof. 2012. Lipid hydration and mobility: an interplay between fluorescence solvent relaxation experiments and molecular dynamics simulations. *Biochimie.* 94:26–32.
17. Halle, B., and L. Nilsson. 2009. Does the dynamic Stokes shift report on slow protein hydration dynamics? *J. Phys. Chem. B.* 113:8210–8213.
18. Barucha-Kraszewska, J., S. Kraszewski, …, M. Hof. 2010. Numerical studies of the membrane fluorescent dyes dynamics in ground and excited states. *Biochim. Biophys. Acta.* 1798:1724–1734.
19. Jurkiewicz, P., A. Olzyńska, …, M. Hof. 2006. Headgroup hydration and mobility of DOTAP/DOPC bilayers: a fluorescence solvent relaxation study. *Langmuir.* 22:8741–8749.
20. Bagatolli, L. A. 2013. Laurdan fluorescence properties in membranes: a journey from the fluorometer to the microscope. *In* Fluorescent Methods to Study Biological Membranes. Y. Mély and G. Duportail, editors. Springer, Berlin, Germany, pp. 3–35.
21. Parasassi, T., F. Conti, and E. Gratton. 1986. Fluorophores in a polar medium: time dependence of emission spectra detected by multifrequency phase and modulation fluorometry. *Cell. Mol. Biol.* 32:99–102.
22. Kwiatek, J. M., E. Hinde, and K. Gaus. 2014. Microscopy approaches to investigate protein dynamics and lipid organization. *Mol. Membr. Biol.* 31:141–151.
23. Parasassi, T., M. Di Stefano, …, E. Gratton. 1994. Cholesterol modifies water concentration and dynamics in phospholipid bilayers: a fluorescence study using Laurdan probe. *Biophys. J.* 66:763–768.
24. Hof, M. 1999. Solvent relaxation in biomembranes. *In* Applied Fluorescence in Chemistry, Biology and Medicine. Springer, Berlin, Germany, pp. 439–456.
25. Jurkiewicz, P. 2007. Fluorescence solvent relaxation technique in biomembranes. PhD thesis, Wrocław University of Technology, Wrocław, Poland.
26. Macháň, R., P. Jurkiewicz, …, M. Hof. 2014. Peripheral and integral membrane binding of peptides characterized by time-dependent fluorescence shifts: focus on antimicrobial peptide LAH_4. *Langmuir.* 30:6171–6179.
27. Jurkiewicz, P., L. Cwiklik, …, M. Hof. 2012. Structure, dynamics, and hydration of POPC/POPS bilayers suspended in NaCl, KCl, and CsCl solutions. *Biochim. Biophys. Acta.* 1818:609–616.
28. Beranova, L., L. Cwiklik, …, P. Jungwirth. 2010. Oxidation changes physical properties of phospholipid bilayers: fluorescence spectroscopy and molecular simulations. *Langmuir.* 26:6140–6144.
29. Pokorna, S., P. Jurkiewicz, …, M. Hof. 2013. Interactions of monovalent salts with cationic lipid bilayers. *Faraday Discuss.* 160:341–358.
30. Först, G., L. Cwiklik, …, M. Hof. 2014. Interactions of β-blockers with model lipid membranes: molecular view of the interaction of acebutolol, oxprenolol, and propranolol with phosphatidylcholine vesicles by time-dependent fluorescence shift and molecular dynamics simulations. *Eur. J. Pharm. Biopharm.* 87:559–569.
31. Sanchez, S. A., M. A. Tricerri, and E. Gratton. 2012. Laurdan generalized polarization fluctuations measures membrane packing microheterogeneity in vivo. *Proc. Natl. Acad. Sci. USA.* 109:7314–7319.
32. Stöckl, M., A. P. Plazzo, …, A. Herrmann. 2008. Detection of lipid domains in model and cell membranes by fluorescence lifetime imaging microscopy of fluorescent lipid analogues. *J. Biol. Chem.* 283:30828–30837.
33. Heberle, F. A., M. Doktorova, …, G. W. Feigenson. 2013. Hybrid and nonhybrid lipids exert common effects on membrane raft size and morphology. *J. Am. Chem. Soc.* 135:14932–14935.
34. Smith, A. K., and J. H. Freed. 2009. Determination of tie-line fields for coexisting lipid phases: an ESR study. *J. Phys. Chem. B.* 113:3957–3971.
35. Heberle, F. A., J. Wu, …, G. W. Feigenson. 2010. Comparison of three ternary lipid bilayer mixtures: FRET and ESR reveal nanodomains. *Biophys. J.* 99:3309–3318.

36. Marushchak, D., N. Gretskaya, …, L. B.-A. Johansson. 2007. Self-aggregation—an intrinsic property of GM_1 in lipid bilayers. *Mol. Membr. Biol.* 24:102–112.

37. Fery-Forgues, S., J.-P. Fayet, and A. Lopez. 1993. Drastic changes in the fluorescence properties of NBD probes with the polarity of the medium: involvement of a TICT state? *J. Photochem. Photobiol. Chem.* 70:229–243.

38. Paprica, P. A., N. C. Baird, and N. O. Petersen. 1993. Theoretical and experimental analyses of optical transitions of nitrobenzoxadiazole (NBD) derivatives. *J. Photochem. Photobiol. Chem.* 70:51–57.

39. Haldar, S., and A. Chattopadhyay. 2013. Application of NBD-labeled lipids in membrane and cell biology. *In* Fluorescent Methods to Study Biological Membranes. Y. Mély and G. Duportail, editors. Springer, Berlin, Germany, pp. 37–50.

40. Chattopadhyay, A., and E. London. 1987. Parallax method for direct measurement of membrane penetration depth utilizing fluorescence quenching by spin-labeled phospholipids. *Biochemistry.* 26:39–45.

41. Huster, D., P. Müller, …, A. Herrmann. 2001. Dynamics of membrane penetration of the fluorescent 7-nitrobenz-2-oxa-1,3-diazol-4-yl (NBD) group attached to an acyl chain of phosphatidylcholine. *Biophys. J.* 80:822–831.

42. Loura, L. M. S., and J. P. P. Ramalho. 2007. Location and dynamics of acyl chain NBD-labeled phosphatidylcholine (NBD-PC) in DPPC bilayers. A molecular dynamics and time-resolved fluorescence anisotropy study. *Biochim. Biophys. Acta.* 1768:467–478.

43. Stöckl, M. T., and A. Herrmann. 2010. Detection of lipid domains in model and cell membranes by fluorescence lifetime imaging microscopy. *Biochim. Biophys. Acta.* 1798:1444–1456.

44. Kaiser, H.-J., D. Lingwood, …, K. Simons. 2009. Order of lipid phases in model and plasma membranes. *Proc. Natl. Acad. Sci. USA.* 106:16645–16650.

45. Sezgin, E., I. Levental, …, P. Schwille. 2012. Partitioning, diffusion, and ligand binding of raft lipid analogs in model and cellular plasma membranes. *Biochim. Biophys. Acta.* 1818:1777–1784.

46. Patel, H., C. Tscheka, …, H. Heerklotz. 2011. All-or-none membrane permeabilization by fengycin-type lipopeptides from *Bacillus subtilis* QST713. *Biochim. Biophys. Acta.* 1808:2000–2008.

47. Imura, Y., N. Choda, and K. Matsuzaki. 2008. Magainin 2 in action: distinct modes of membrane permeabilization in living bacterial and mammalian cells. *Biophys. J.* 95:5757–5765.

48. Pokorny, A., L. E. Yandek, …, P. F. F. Almeida. 2006. Temperature and composition dependence of the interaction of δ-lysin with ternary mixtures of sphingomyelin/cholesterol/POPC. *Biophys. J.* 91:2184–2197.

49. Heerklotz, H., and J. Seelig. 2007. Leakage and lysis of lipid membranes induced by the lipopeptide surfactin. *Eur. Biophys. J.* 36:305–314.

50. Gregory, S. M., A. Pokorny, and P. F. F. Almeida. 2009. Magainin 2 revisited: a test of the quantitative model for the all-or-none permeabilization of phospholipid vesicles. *Biophys. J.* 96:116–131.

51. Clayton, A. H. A. 2008. The polarized AB plot for the frequency-domain analysis and representation of fluorophore rotation and resonance energy homotransfer. *J. Microsc.* 232:306–312.

52. van Rooijen, B. D., M. M. A. E. Claessens, and V. Subramaniam. 2010. Membrane permeabilization by oligomeric α-synuclein: in search of the mechanism. *PLoS ONE.* 5:e14292.

53. Tamba, Y., and M. Yamazaki. 2005. Single giant unilamellar vesicle method reveals effect of antimicrobial peptide magainin 2 on membrane permeability. *Biochemistry.* 44:15823–15833.

54. Fuertes, G., A. J. García-Sáez, …, J. Salgado. 2010. Pores formed by Baxα5 relax to a smaller size and keep at equilibrium. *Biophys. J.* 99:2917–2925.

55. Kristensen, K., J. R. Henriksen, and T. L. Andresen. 2014. Quantification of leakage from large unilamellar lipid vesicles by fluorescence correlation spectroscopy. *Biochim. Biophys. Acta.* 1838:2994–3002.

56. Ladokhin, A. S., W. C. Wimley, and S. H. White. 1995. Leakage of membrane vesicle contents: determination of mechanism using fluorescence requenching. *Biophys. J.* 69:1964–1971.

57. Schwarz, G., and C. H. Robert. 1990. Pore formation kinetics in membranes, determined from the release of marker molecules out of liposomes or cells. *Biophys. J.* 58:577–583.

58. Schwarz, G. 1995. Pore kinetics reflected in the dequenching of a lipid vesicle entrapped fluorescent dye. *Biochim. Biophys. Acta.* 1239:51–57.

59. Arbuzova, A., and G. Schwarz. 1999. Pore-forming action of mastoparan peptides on liposomes: a quantitative analysis. *Biochim. Biophys. Acta.* 1420:139–152.

60. Gregory, S. M., A. Cavenaugh, …, P. F. F. Almeida. 2008. A quantitative model for the all-or-none permeabilization of phospholipid vesicles by the antimicrobial peptide cecropin A. *Biophys. J.* 94: 1667–1680.

61. Patel, H., C. Tscheka, and H. Heerklotz. 2009. Characterizing vesicle leakage by fluorescence lifetime measurements. *Soft Matter.* 5:2849–2851.

62. Lakowicz, J. R. 2006. Principles of Fluorescence Spectroscopy, 3rd Ed. Springer Science+Business Media, New York.

63. Baumann, J., and M. D. Fayer. 1986. Excitation transfer in disordered two-dimensional and anisotropic three-dimensional systems: effects of spatial geometry on time-resolved observables. *J. Chem. Phys.* 85:4087.

64. Shi, J., T. Yang, …, P. S. Cremer. 2007. GM_1 clustering inhibits cholera toxin binding in supported phospholipid membranes. *J. Am. Chem. Soc.* 129:5954–5961.

65. Göttfert, F., C. A. Wurm, …, S. W. Hell. 2013. Coaligned dual-channel STED nanoscopy and molecular diffusion analysis at 20 nm resolution. *Biophys. J.* 105:L01–L03.

66. Sachl, R., J. Humpolíčková, …, M. Hof. 2011. Limitations of electronic energy transfer in the determination of lipid nanodomain sizes. *Biophys. J.* 101:L60–L62.

67. de Almeida, R. F. M., L. M. S. Loura, …, M. Prieto. 2005. Lipid rafts have different sizes depending on membrane composition: a time-resolved fluorescence resonance energy transfer study. *J. Mol. Biol.* 346:1109–1120.

68. Loura, L. M. S., and M. Prieto. 2000. Resonance energy transfer in heterogeneous planar and bilayer systems: theory and simulation. *J. Phys. Chem. B.* 104:6911–6919.

69. Loura, L. M. S., A. Fedorov, and M. Prieto. 2001. Fluid-fluid membrane microheterogeneity: a fluorescence resonance energy transfer study. *Biophys. J.* 80:776–788.

70. Engström, S., M. Lindberg, and L. B.-A. Johansson. 1988. Monte Carlo simulations of electronic energy transfer in three-dimensional systems: a comparison with analytical theories. *J. Chem. Phys.* 89:204.

71. Štefl, M., R. Šachl, …, M. Hof. 2012. Dynamics and size of cross-linking-induced lipid nanodomains in model membranes. *Biophys. J.* 102:2104–2113.

72. Sachl, R., M. Amaro, …, M. Hof. 2014. On multivalent receptor activity of GM_1 in cholesterol containing membranes. *Biochim. Biophys. Acta.* [Epub ahead of print]. http://dx.doi.org/10.1016/j.bbamcr.2014.07.016.

73. Castro, B. M., R. F. M. de Almeida, …, M. Prieto. 2012. The photophysics of a rhodamine head-labeled phospholipid in the identification and characterization of membrane lipid phases. *Chem. Phys. Lipids.* 165:311–319.

74. Medhage, B., E. Mukhtar, …, J. G. Molotkovsky. 1992. Electronic energy transfer in anisotropic systems. Part 5. Rhodamine-lipid derivatives in model membranes. *J. Chem. Soc., Faraday Trans.* 88:2845.

75. Bader, A. N., S. Hoetzl, …, H. C. Gerritsen. 2011. Homo-FRET imaging as a tool to quantify protein and lipid clustering. *ChemPhysChem.* 12:475–483.

76. Runnels, L. W., and S. F. Scarlata. 1995. Theory and application of fluorescence homotransfer to melittin oligomerization. *Biophys. J.* 69:1569–1583.

77. Berberan-Santos, M. N., and B. Valeur. 1991. Fluorescence depolarization by electronic energy transfer in donor–acceptor pairs of like and unlike chromophores. *J. Chem. Phys.* 95:8048–8055.

78. Yeow, E. K. L., and A. H. Clayton. 2007. Enumeration of oligomerization states of membrane proteins in living cells by homo-FRET spectroscopy and microscopy: theory and application. *Biophys. J.* 92:3098–3104.

79. Melo, A. M., A. Fedorov, …, A. Coutinho. 2014. Exploring homo-FRET to quantify the oligomer stoichiometry of membrane-bound proteins involved in a cooperative partition equilibrium. *Phys. Chem. Chem. Phys.* 16:18105–18117.

80. Sachl, R., I. Boldyrev, and L. B.-A. Johansson. 2010. Localization of BODIPY-labeled phosphatidylcholines in lipid bilayers. *Phys. Chem. Chem. Phys.* 12:6027–6034.

81. Loura, L. M. S., A. Coutinho, …, M. Prieto. 2006. Structural effects of a basic peptide on the organization of dipalmitoylphosphatidylcholine/dipalmitoylphosphatidylserine membranes: a fluorescent resonance energy transfer study. *J. Phys. Chem. B.* 110:8130–8141.

82. Coutinho, A., L. M. S. Loura, …, M. Prieto. 2008. Pinched multilamellar structure of aggregates of lysozyme and phosphatidylserine-containing membranes revealed by FRET. *Biophys. J.* 95:4726–4736.